analytical chemistry

pubs.acs.org/ac Article

Construction of a Polarity-Switchable Photoelectrochemical Biosensor for Ultrasensitive Detection of miRNA-141

Xiankang Niu, Changtong Lu, Dan Su, Fang Wang, Weihong Tan, and Fengli Qu*

Cite This: *Anal. Chem.* 2021, 93, 13727−13733 Read Online

ACCESS | Metrics & More | Article Recommendations | Supporting Information

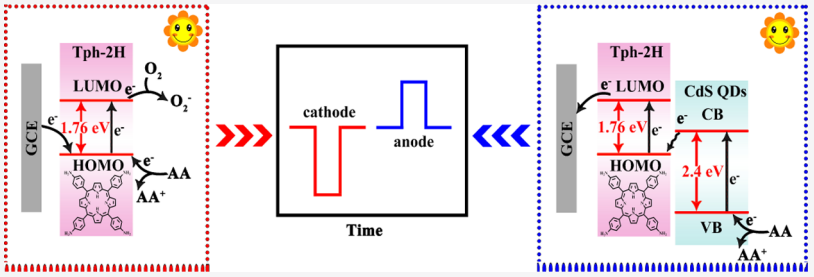

ABSTRACT: As an early-stage tumor biomarker, microRNA (miRNA) has clinical application potential and its sensitive and accurate detection is significant for early tumor diagnosis. In this study, a photoelectrochemical (PEC) biosensing platform was fabricated for ultrasensitive miRNA-141 detection, which is based on a photocurrent polarity-switchable system using CdS quantum dots (QDs) in the presence of a 5,10,15,20-tetrakis (4-aminophenyl)-21H,23H-porphine (Tph-2H)-coated glassy carbon electrode (GCE). As an excellent photoactive material, Tph-2H has a narrow band gap that effectively gathers photoelectrons under visible light irradiation and improves the transfer ability of photogenerated electrons. Further, the detection sensitivity of miRNA-141 could be significantly improved by combining an enzyme-assisted recycle amplification reaction and a magnetic bead-based separation strategy. The proposed photocurrent polarity-switchable PEC biosensor could efficiently eliminate the false-positive or false-negative signals and achieve a wide linear response range from 1 fM to 1 nM with a low detection limit of 0.33 fM for miRNA-141, providing a potentially alternative solution for detecting other biomarkers in bioanalysis and clinical diagnosis.

INTRODUCTION

MicroRNA-141 (miRNA-141) is one of the most important cancer biomarkers. Its sensitive and accurate detection is highly significant for the early diagnosis and prognosis of ovarian, hepatocellular, and prostate cancers clinically.[1−5] To date, various effective analytical methods have been proposed, such as electrochemistry (EC),[6] fluorimetry (FL),[7] electrochemiluminescence (ECL),[8] surface plasmon resonance (SPR),[9] and surface colorimetry (CL).[10] Although these methods achieve a certain degree of detection of miRNA-141, nevertheless, which are usually limited by high cost, complex sample processing, incorporating toxic reagents, and high background signals. Recently, photoelectrochemical (PEC) biosensing platform, an emerging and developing analytical technique, has provided new insights into the detection of miRNA. PEC biosensing has attracted extensive attention in the field of analysis due to its advantages in terms of simple device, easy operation, outstanding stability, ultrahigh sensitivity, and low background signal.[11−15] Therefore, developing an ultrasensitive and highly selective PEC biosensing platform for detecting miRNA-141 is indispensable for early medical diagnosis of relevant diseases.

By far, in terms of PEC response methods, "signal-on" and "signal-off" are two types of major detection strategy. Chai et al. developed a signal-off PEC biosensor for the ultrasensitive detection of miRNA-141 by combining CdTe quantum dot (QD)-CeO_2 complex-based target converting amplification and DNA supersandwich amplification.[16] Fu et al. designed a signal-on PEC aptasensor for detecting miRNA-141 based on the cascaded quadratic amplification strategy.[17] Generally, the detection limit and sensitivity of the signal-off PEC biosensors are restricted by high background signals. Thus, the signal-on PEC biosensors were more conducive to detecting targets with high sensitivity and accuracy. However, the elimination of the influence of false-positive or false-negative signals on the test environment still faced severe challenges, which mainly arose from the possible oxidative or reductive interferents in complex samples or detection substrates.[18] Recently, a novel photocurrent signal-reversal mode was developed by the intercalation of methylene blue into CdTe QDs-dsDNA-Fe_3O_4@SiO_2 composites.[19] The polarity-switching mode, as a novel type of

Received: August 12, 2021
Accepted: September 17, 2021
Published: October 1, 2021

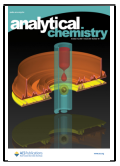

https://doi.org/10.1021/acs.analchem.1c03460
Anal. Chem. 2021, 93, 13727−13733

Scheme 1. Schematic Description of the Proposed PEC Biosensor for miRNA-141 Detection: T7 Exonuclease-Assisted Target Recycle Amplification Process (A) and Mechanism of Electron Transfer for Cathode Photocurrent Generation (B) and Anode Photocurrent Generation (C)

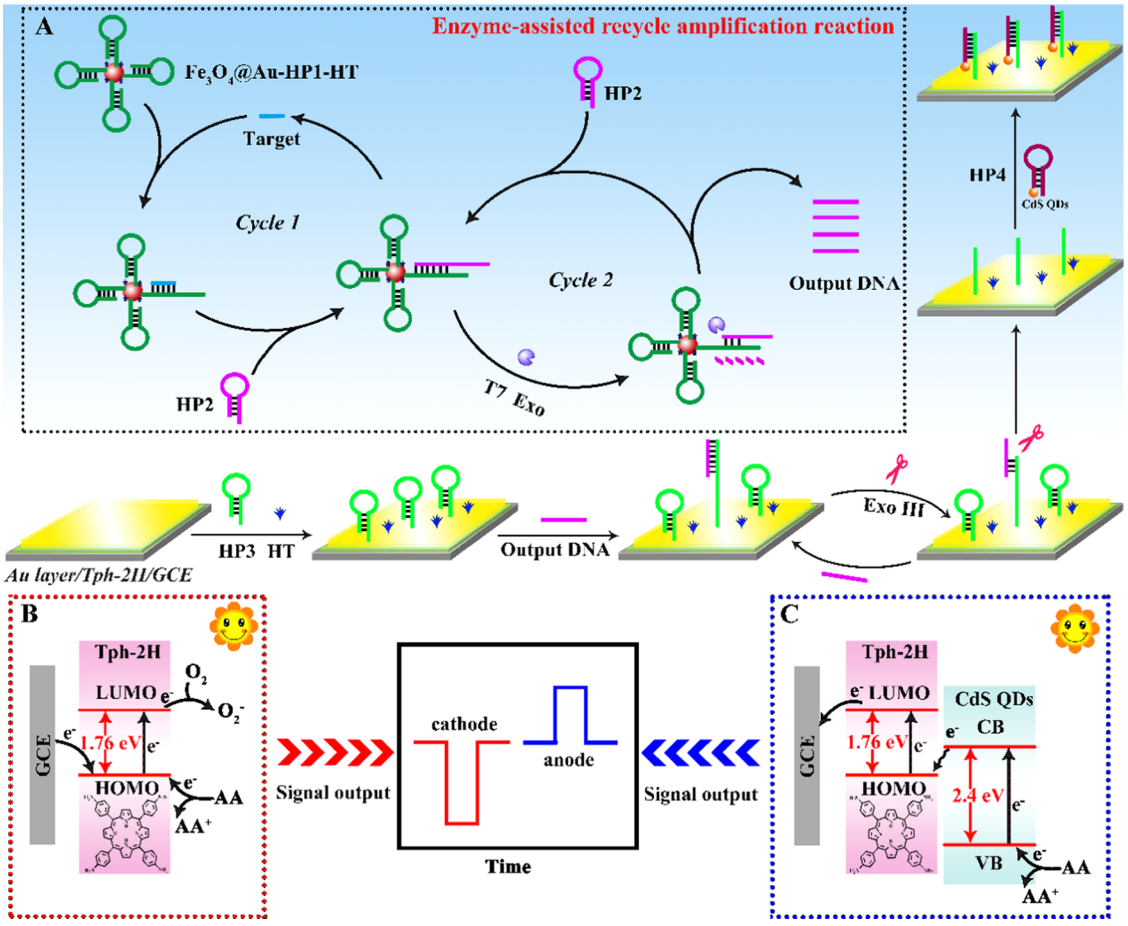

signal expression in its infancy, provided a new perspective for constructing PEC biosensors. The aforementioned polarity-switching PEC biosensors were constructed based on various semiconductive materials such as CdTe QDs, CdSe QDs, and $AgInS_2$ semiconductors. The photo-to-current conversion efficiency still needed to be improved in that their absorption wave range was mainly concentrated in the near-ultraviolet light region.[20,21] Exhilaratingly, absorption of the organic functional molecular material 5,10,15,20-tetrakis (4-aminophenyl)-21H,23H-porphine (Tph-2H) could be extended from the ultraviolet absorption spectrum to the long-wave region due to the π electron conjugated system, indicating that Tph-2H had a good light-harvesting ability. Besides, Tph-2H with a narrow band gap (1.7 eV)[22] was an excellent photoelectrically active material that could efficiently gather photoelectrons under visible light excitation, enabling the efficient promotion of photonics transfer capability, thereby dramatically improving the photoelectric conversion efficiency.[23,24] Based on these advantages, Tph-2H exhibited potential to be used in developing a PEC biosensor to achieve ultrasensitive and highly selective detection of miRNA-141.

Inspired by the above developments, in this study, a signal-switchable-mode PEC biosensor for ultrasensitive and highly selective detection of miRNA-141 was developed by introducing CdS QDs to the Tph-2H-coated glassy carbon electrode (GCE). By combining organic molecular materials with inorganic semiconductor materials, the present study proposed a signal polarity-switching system that was of considerable advantage to boost the sensitivity and selectivity of the PEC biosensor. As shown in Scheme 1, the photoactive material Tph-2H was immobilized on the GCE to provide an initial cathode photocurrent. In the presence of the target, output DNA was released due to the single-enzyme-assisted double-cycle amplification reaction and strand-displacement strategy. Subsequently, the output DNA hybridized with hairpin DNA 3 (HP3), which was modified on the surface of Au layer/Tph-2H/GCE *via* Au−S bonds. Then, the HP3/output DNA duplex was cleaved to release output DNA once again with the assistance of Exo III, further increasing the detection range of the miRNA-141. Ultimately, the hairpin DNA 4 (HP4) with CdS QDs was introduced into the surface of the modified electrode, causing generation of a strong anodic photocurrent. The unique design of the PEC platform enabling ultrasensitive detection of miRNA-141 in complex environmental systems may provide a new perspective for bioanalysis and disease diagnosis and show substantial potential in clinical application.

EXPERIMENTAL SECTION

Preparation Process of Fe_3O_4@Au, CdS QDs, and the Tph-2H Solution. Fe_3O_4@Au was prepared according to a previous report.[24] Briefly, the prepared gold nanoparticles were mixed with Fe_3O_4-NH_2 magnetic microspheres overnight to obtain Fe_3O_4@Au. CdS QDs were synthesized according to a

https://doi.org/10.1021/acs.analchem.1c03460
Anal. Chem. 2021, 93, 13727−13733

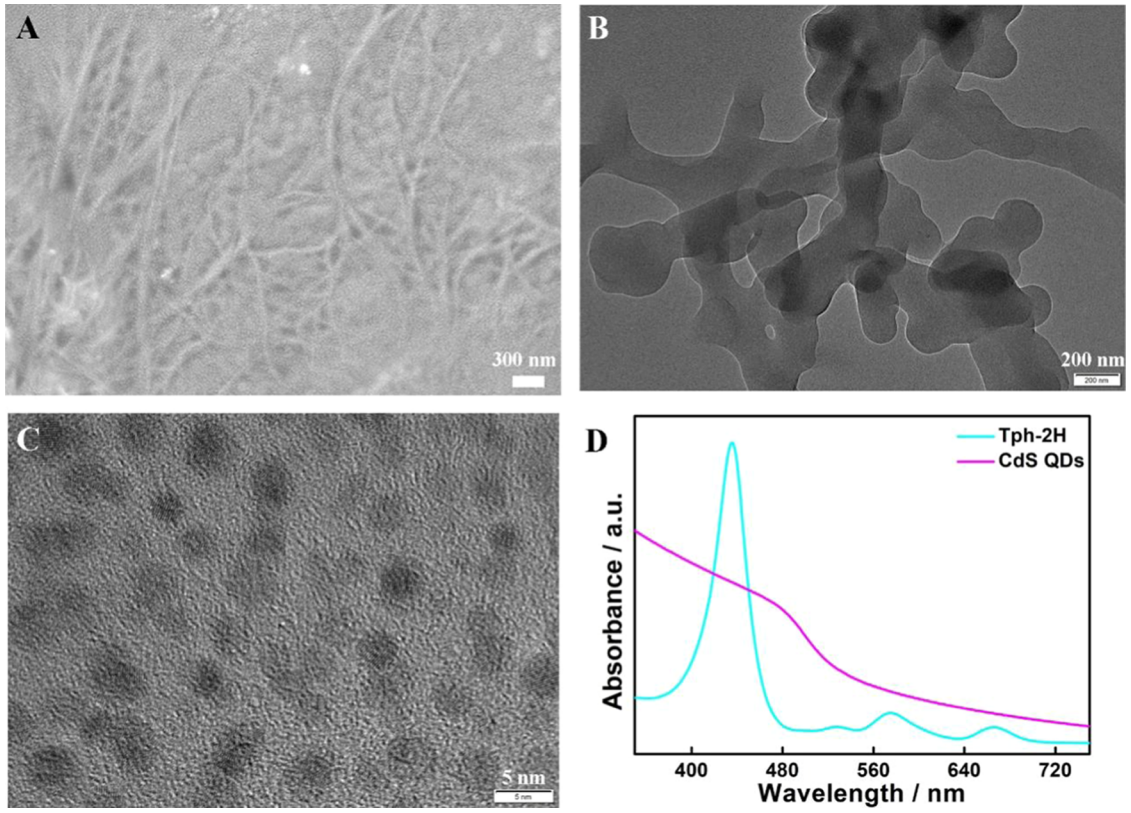

Figure 1. SEM image of Tph-2H (A). TEM image of Tph-2H (B) and HRTEM image of CdS QDs (C). Ultraviolet−visible (UV−vis) absorption spectra of Tph-2H and CdS QDs (D).

previous study with some modifications.[25] First, 0.71 mM $CdCl_2 \cdot 2.5H_2O$ was dissolved in 30 mL of ultrapure water and the mixture was heated to 70 °C. Then, a freshly prepared Na_2S (30 mL, 0.0627 g/mL) solution was slowly injected into the mixture solution and kept at 70 °C for 3 h with continuous stirring. The color of the reaction solution rapidly turned orange-yellow. Next, the obtained orange-yellow solution was centrifuged and washed several times with ultrapure water and ethanol. Eventually, the CdS QDs were redispersed in ultrapure water and stored at 4 °C in the dark for further use. For preparation of the Tph-2H solution, 0.1 mg of Tph-2H was dissolved in 1 mL of *N*,*N*-dimethylformamide and subjected to ultrasonication until a uniform brown-green solution appeared. Finally, the obtained Tph-2H solution was kept at room temperature.

Enzyme-Assisted Signal Amplification for Detection of miRNA-141. The enzyme-assisted signal amplification strategy is depicted in Scheme 1A. First, 250 μL of Fe_3O_4@Au was mixed with 250 μL of 2.5 μM hairpin DNA 1 (HP1) under stirring at 4 °C for 16 h to prepare Fe_3O_4@Au-HP1. Second, the composite was extracted by magnetic separation in the presence of an external magnetic field and redispersed in 200 μL of 0.1 M phosphate buffer solution (PBS, pH 7.4), and 20 μL of 0.1 mM hexanethiol (HT) was introduced into the mixture solution for blocking nonspecific adsorption sites. Third, 100 μL of the target was injected into a solution of Fe_3O_4@Au-HP1-HT and kept at 37 °C for 40 min to form a heteroduplex of HP1/target on the Fe_3O_4@Au surface. Fourth, HP2 (200 μL, 2.5 μM) was appended to the aforementioned solution and then incubated at 37 °C for 2 h. The HP2 strand could compete with the target to form a HP1/HP2 heteroduplex, thereby realizing the release and reuse of the target. Fifth, 60 μL of 10× NEBuffer 4 and 20 μL of T7 exonuclease (1 U/μL) were added to the aforementioned solution. The mixture with a total volume of 600 μL was incubated at 25 °C for 3 h to accomplish the release of the output DNA process, and soon afterward, the enzyme in the system was inactivated *via* incubation at 80 °C for 20 min. Specifically, the unlocked HP1, as a mimic target, was able to hybridize with HP2, which could produce large quantities of output DNA by T7 exonuclease. Finally, the product was collected by magnetic separation for further modification of the PEC biosensor.

Construction of the Biosensor. Before modification, the bare GCE was completely burnished with alumina powder and then sonicated several times in ethanol and ultrapure water.[26] Briefly, 10 μL of Tph-2H was coated on the surface of the bare GCE and dried at 37 °C to acquire a layer of a thin film. Subsequently, gold nanoparticles (Au NPs) were incubated on the modified electrode at 37 °C for 4 h to obtain the Au layer that could covalently connect with Tph-2H by Au−N bonds. On account of the strong interaction of Au−S bonds, 15 μL of HP3 (3 μM) was dropped on the modified electrode surface at 4 °C for 12 h to ensure that HP3 was effectively fixed on the modified electrode. Then, 10 μL of 0.1 mM HT, as a sealing agent, was decorated on the surface of the modified electrode for 35 min to block nonspecific sites. Then, 15 μL of the preceding output DNA was incubated on the modified electrode at 37 °C for 2 h by hybridizing with HP3. A preprepared exonuclease III (Exo III) solution [including 1.5 μL of Exo III (20 U/μL), 1.5 μL of 10× NEBuffer 1, and 12 μL of 0.1 M PBS (pH 7.4)] was sequentially incubated on the modified electrode at 37 °C for 1 h and then deactivated *via* heating at 80 °C for 20 min. In the presence of Exo III, the

https://doi.org/10.1021/acs.analchem.1c03460
Anal. Chem. 2021, 93, 13727−13733

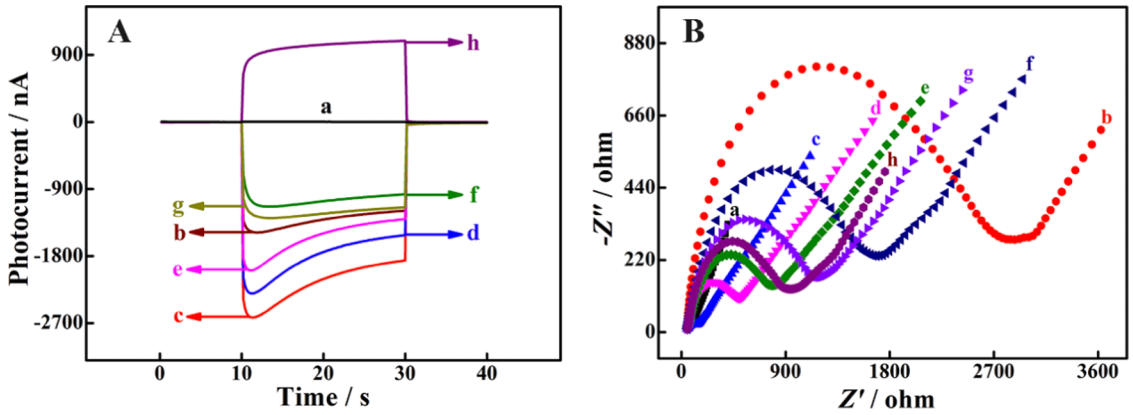

Figure 2. PEC responses (A) and EIS (B) of bare GCE (a), Tph-2H/GCE (b), Au layer/Tph-2H/GCE (c), HP3/Au layer/Tph-2H/GCE (d), HT/HP3/Au layer/Tph-2H/GCE (e), output DNA/HT/HP3/Au layer/Tph-2H/GCE (f), Exo III/output DNA/HT/HP3/Au layer/Tph-2H/GCE (g), and HP4-CdS QDs/Exo III/output DNA/HT/HP3/Au layer/Tph-2H/GCE (h).

HP3/output DNA heteroduplex was cut into a single-stranded DNA, which was a part of the capture DNA. Finally, HP4 with CdS QDs was incubated on the modified electrode surface at 37 °C for 2 h to achieve hybridization with the single-stranded DNA. After each step of electrode modification, the modified GCE was rinsed with ultrapure water to remove the physically absorbed samples. Construction of the PEC biosensor is clearly shown in Scheme 1.

RESULTS AND DISCUSSION

Mechanism of Photoelectron Transfer. The possible photocurrent-generating mechanism is displayed in Scheme 1B,C. The electrons of Tph-2H migrated from their highest occupied molecular orbital (HOMO) to their lowest unoccupied molecular orbital (LUMO) with 460 nm light excitation and then transferred to the dissolved O_2 molecules (electron acceptor) in the electrolyte solution. Subsequently, the photogenerated holes (h^+) could accept electrons from the GCE surface and ascorbic acid (AA) for reducing the recombination of electrons and holes to obtain an initial photocathode signal (Scheme 1B).[27−29] The target was converted into DNA products, triggering a series of DNA reactions to introduce CdS QDs into the modified electrode surface *via* the enzyme-assisted recycle amplification reaction and the strand-displacement strategy because of the existence of miRNA-141 (target). As shown in Scheme 1C, the feasible mechanism for the PEC signal-switchable-system of the modified electrode was as follows. Under visible light, the photoelectrons of CdS QDs transited from the valence band (VB) to the conduction band (CB). The photoelectrons were transferred from the CB of CdS QDs to the HOMO of Tph-2H and ultimately reached the surface of the GCE due to excellent energy-level matching. The h^+ at the VB of CdS QDs was consumed by the reducing substance AA in the electrolyte solution, generating a distinct anodic PEC signal.[30] On account of the reverse polarity of the photocurrent between the Tph-2H/GCE and CdS QDs/Tph-2H/GCE electrodes, the developed PEC biosensor possessed the superiority of negative background signals that made the biosensor exhibit high selectivity and sensitivity for miRNA-141 analysis.

Characterizations of Tph-2H and CdS QDs. The morphologies of Tph-2H and CdS QDs were characterized using scanning electron microscopy (SEM), Transmission electron microscopy (TEM) and high-resolution transmission electron microscopy (HRTEM), respectively. The SEM image of Tph-2H with a wrinkled film structure is illustrated in Figure 1A. As observed in Figure 1B, Tph-2H possessed a net structure with a width of about 170 nm owing to its excellent film-forming ability. As shown in Figure 1C, CdS QDs had a clear crystal lattice structure and good distribution, and their average diameter was around 3 nm. The UV−vis absorption spectras are presented in Figure 1D. Tph-2H had one strong absorption peak at 460 nm and two minor weak absorption peaks at 570 and 660 nm, which was in accordance with a previous study.[22] The broad absorption of Tph-2H in the UV−vis region showed that it had outstanding light-capture capability. Moreover, CdS QDs exhibited a wide absorption range in the UV−vis light region, meaning that CdS QDs were adequate photoelectrode materials.[21] The aforementioned results demonstrated the successful preparation of Tph-2H and CdS QDs.

PEC and EIS Characterization of the Constructed Biosensor. The photocurrent signals and electrochemical impedance spectroscopy (EIS) of the assembly procedure were characterized to verify the successful construction of the proposed biosensor. As exhibited in Figure 2A, a strongly enhanced cathodic photocurrent was obtained for the Tph-2H-modified electrode compared with the photocurrent response of bare GCE (curve a), which was attributed to the excellent photoelectric activity of Tph-2H (curve b). As Au NPs were introduced into the modified electrode surface *via* Au−N bonds, an enhanced photocurrent intensity (curve c) was obtained owing to its outstanding conductivity. With HP3 (curve d), HT (curve e), and output DNA (curve f) ceaselessly immobilized on the modified electrode, the photocurrent signal weakened successively by virtue of its poor charge-transfer ability. However, after decorating Exo III on the modified GCE, the photocurrent response (curve g) was slightly enhanced due to the lessened steric hindrance. Ultimately, an anodic PEC response (curve h) was observed when HP4-CdS QDs were introduced into the modified electrode. Meanwhile, to further validate the successful stepwise assembly procedure of the PEC biosensor, EIS measurements (Figure 2B) were conducted in 2 mL of PBS containing 5.0 mM $K_3[Fe(CN)_6]/K_4[Fe(CN)_6]$ (1:1) and 0.1 M KCl. The Tph-2H-modified electrode exhibited a greater charge-transfer resistance (R_{et}) (curve b) than bare GCE (curve a), due to the poor conductivity of the Tph-2H film,

https://doi.org/10.1021/acs.analchem.1c03460
Anal. Chem. 2021, 93, 13727−13733

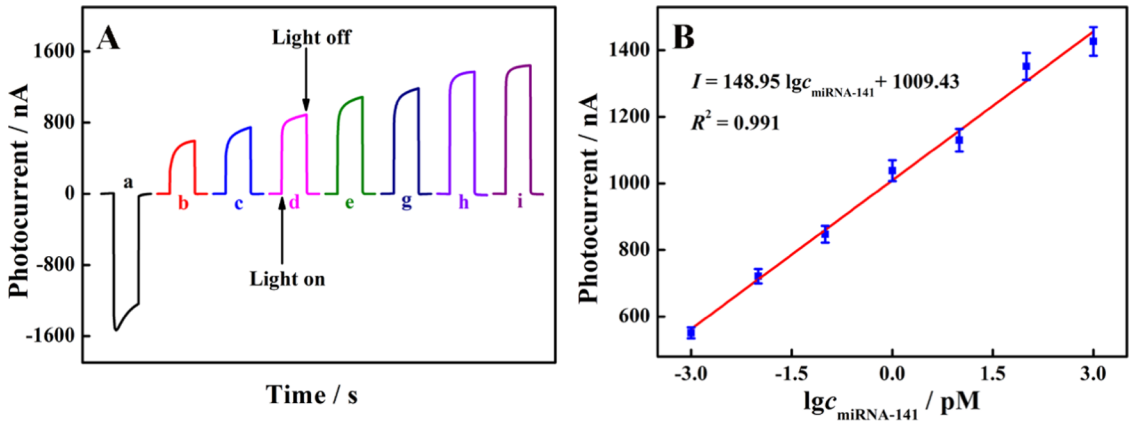

Figure 3. (A) Photocurrent responses of the PEC biosensor with different concentrations of miRNA-141: 0, 1 fM, 10 fM, 100 fM, 1 pM, 10 pM, 100 pM, and 1 nM. (B) Calibration curve between photocurrent and the logarithm of miRNA-141 concentration.

which could impede the photoelectron transfer. After Au NPs were immobilized on the electrode surface, a reduced R_{et} (curve c) was obtained due to the excellent conductivity of Au NPs. After stepwise modification of HP3, HT, output DNA, and HP4, the R_{et} value increased successively because of the electrostatic repulsion and poor conductivity, which could hinder the photoelectron transfer process of the redox reaction on the modified electrode surface (curves d, e, and f). When Exo III was decorated on GCE, the R_{et} value decreased due to the steric hindrance of the modified electrode (curve g). Eventually, an obviously reduced R_{et} value was acquired (curve h) compared with that of curve g by virtue of the introduction of HP4-CdS QDs, which was attributed to the superior electrochemical activity of CdS QDs. These results indicated the successful construction of the proposed PEC biosensor.

Detection Performance of the Biosensor. The photocurrent signals were monitored for a series of miRNA-141 concentrations under optimal experimental conditions (Figure S1, Supporting Information) to investigate the analytical performance of the presented PEC biosensor. According to Figure 3A, a cathodic photocurrent was obtained without the target (miRNA-141). However, in the presence of miRNA-141 (1 fM), the cathodic photocurrent switched to the anodic photocurrent, when the PEC response was 551.5 nA. The value of the anodic photocurrent increased with enhancement in the concentration of miRNA-141. Notably, the background signal was cathodic photocurrent, whereas the PEC response signal was anodic photocurrent. The background signal could be eliminated completely by assessing the relationship between the concentrations of miRNA-141 and the values of the anodic photocurrents, endowing the PEC biosensor with eminent sensitivity. As shown in Figure 3B, a linear relationship between the concentrations of miRNA-141 and the values of the anodic photocurrents could be monitored from 1 fM to 1 nM, and the linear equation was I = 148.95 lg c + 1009.43 (R^2 = 0.991) with a detection limit of 0.33 fM (S/N = 3). Compared with the results of previous studies, the constructed PEC aptasensor displayed excellent potential and analytical performance for ultrasensitive detection of miRNA-141 (Table 1).

Specificity and Stability of the Proposed Biosensor. To probe the specificity and selectivity of the constructed biosensor, miRNA-21, miRNA-155, miRNA-182-5p, and miRNA-122 as the possible interfering substances were, respectively, contrasted with miRNA-141. As observed in Figure 4A, strong cathodic photocurrents were monitored in the presence of 500 pM interferents, and all of the obtained cathodic photocurrents were slightly lower than those detected for the blank group because of the possible slight adsorption of the interferents on the modified electrode. However, the introduction of 5 pM miRNA-141 generated an intense anodic photocurrent, meaning that only the presence of miRNA-141 could produce an anodic photocurrent and the aforementioned interferents merely led to a cathodic photocurrent. Moreover, an anodic photocurrent was also monitored in the mixture component, containing miRNA-141 (5 pM) and all of the aforementioned interferents (the concentration of each interferent was 500 pM), yet the value of the anodic photocurrent was slightly lower than that in the miRNA-141 sample without interferents. Simultaneously, the PEC signals of the proposed biosensor revealed no distinct changes in 1 pM miRNA-141 under successive "off−on−off" light for 13 cycles, and the relative standard deviation (RSD) was 0.47% (Figure 4B), indicating that the developed biosensor had excellent stability during the analysis.

Table 1. Comparison of Other Studies with Our Present Method for miRNA Detection

analytical method	detection range	limit of detection	references
fluorescent	1 pM to 2.5 nM	0.21 pM	31
fluorescent	25 pM to 10 nM	16.5 pM	32
fluorescent	200 fM to 50 pM	67.3 fM	33
SPR	0 to 50 pM	1 fM	34
ECL	10 fM to 100 pM	3.3 fM	35
PEC	350 fM to 5 nM	153 fM	36
PEC	1 fM to 10 pM	0.5 fM	37
PEC	1 fM to 1 nM	0.33 fM	present study

Detection of miRNA-141 in Clinical Serum Samples. The PEC biosensor was used for analyzing miRNA-141 in serum samples of healthy people to estimate the feasibility and potential application. The target with different concentrations was spiked into 50-fold diluted clinical serum samples of healthy people for further observation. As exhibited in Table S2 (Supporting Information), the recoveries were 99.3−104.9% with an RSD of 1.5−2.6% (n = 3), which demonstrated that the developed aptasensor had potential applications in real clinical samples.

https://doi.org/10.1021/acs.analchem.1c03460
Anal. Chem. 2021, 93, 13727−13733

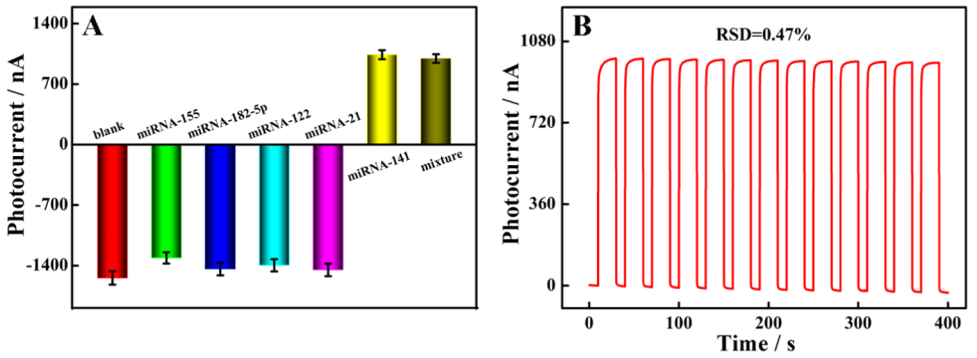

Figure 4. (A) Specificity of the constructed PEC biosensor toward different detection samples: blank, miRNA-155 (500 pM), miRNA-182-5p (500 pM), miRNA-122 (500 pM), miRNA-21 (500 pM), miRNA-141 (5 pM), and the mixture containing miRNA-141 (5 pM) and four interferents (the concentration of each interferent, 500 pM). (B) Stability of the proposed biosensor under serial off−on−off light for 13 cycles.

CONCLUSIONS

In summary, a signal-switchable-mode PEC biosensor for ultrasensitive detection of miRNA-141 was established by introducing CdS QDs to the excellent photoactive Tph-2H-coated GCE. Besides, the developed PEC biosensor displayed prominent analytical performance with a wide detection range (1 fM−1 nM) and a low detection limit of 0.33 fM owing to the target-triggered enzyme-assisted cycle amplification reaction and the polarity-switchable strategy. Furthermore, the proposed PEC biosensing platform could differentiate target miRNA-141 from other microRNA and exhibited outstanding stability and high sensitivity that could be easily extended to detect various low-abundance miRNAs. On account of the outstanding anti-interference ability and complete elimination of the influence of negative background signals, the proposed polarity-switchable system provides a new way for early analysis and diagnosis of cancer in clinics.

ASSOCIATED CONTENT

Supporting Information

The Supporting Information is available free of charge at https://pubs.acs.org/doi/10.1021/acs.analchem.1c03460.

Materials and reagents and sequences used in the experiment (Table S1); apparatus, PEC measurement, Native PAGE Analysis Process, and condition optimization (Figure S1); and PAGE analysis (Figure S2) and recovery assay of miRNA-141 in the clinical serum samples (Table S2) (PDF)

AUTHOR INFORMATION

Corresponding Author

Fengli Qu − *Department of Pathology, Cancer Hospital of the University of Chinese Academy of Sciences, Institute of Basic Medicine and Cancer, Chinese Academy of Sciences, Hangzhou 310022 Zhejiang, China; College of Chemistry and Chemical Engineering, Qufu Normal University, Qufu 273165 Shandong, China;* orcid.org/0000-0001-6311-3051; Phone: +86 537 4456301.; Email: fengliquhn@hotmail.com; Fax: (+86) 537-4456301

Authors

Xiankang Niu − *Department of Pathology, Cancer Hospital of the University of Chinese Academy of Sciences, Institute of Basic Medicine and Cancer, Chinese Academy of Sciences, Hangzhou 310022 Zhejiang, China; College of Chemistry and Chemical Engineering, Qufu Normal University, Qufu 273165 Shandong, China*

Changtong Lu − *College of Chemistry and Chemical Engineering, Qufu Normal University, Qufu 273165 Shandong, China*

Dan Su − *Department of Pathology, Cancer Hospital of the University of Chinese Academy of Sciences, Institute of Basic Medicine and Cancer, Chinese Academy of Sciences, Hangzhou 310022 Zhejiang, China*

Fang Wang − *College of Chemistry and Chemical Engineering, Qufu Normal University, Qufu 273165 Shandong, China*

Weihong Tan − *Department of Pathology, Cancer Hospital of the University of Chinese Academy of Sciences, Institute of Basic Medicine and Cancer, Chinese Academy of Sciences, Hangzhou 310022 Zhejiang, China;* orcid.org/0000-0002-8066-1524

Complete contact information is available at: https://pubs.acs.org/10.1021/acs.analchem.1c03460

Notes

The authors declare no competing financial interest.

ACKNOWLEDGMENTS

This work was financially supported by the National Natural Science Foundation of China (21775089 and 22074080), Changjiang Scholar Program of the Ministry of Education of China (Q2019258), and the Taishan Scholar Program of Shandong Province (tsqn201909106).

REFERENCES

(1) Calin, G. A.; Croce, C. M. *Nat. Rev. Cancer.* **2006**, *6*, 857−866.
(2) He, L.; Hannon, G. J. *Nat. Rev. Genet.* **2004**, *5*, 522−531.
(3) Xu, Z. H.; Wang, H.; Wang, J.; Zhao, W.; Xu, J. J.; Chen, H. Y. *Anal. Chem.* **2019**, *91*, 12000−12005.
(4) Jou, A. F.; Lu, C. H.; Ou, Y. C.; Wang, S. S.; Hsu, S. L.; Willner, I.; Ho, J. A. A. *Chem. Sci.* **2015**, *6*, 659−665.
(5) Nie, Y. M.; Zhang, P.; Wang, H. J.; Zhuo, Y.; Chai, Y.; Yuan, R. *Anal. Chem.* **2017**, *89*, 12821−12827.
(6) Liu, L.; Deng, D. H.; Wu, D. H.; Hou, W. L.; Wang, L.; Li, N.; Sun, Z. F. *Anal. Chim. Acta.* **2021**, *1149*, No. 338199.
(7) Chen, J. L.; Yan, J.; Feng, Q. M.; Miao, X. M.; Dou, B. T.; Wang, P. *Biosens. Bioelectron.* **2021**, *176*, No. 112955.
(8) Wang, C.; Han, Q.; Mo, F. J.; Chen, M.; Xiong, Z. W.; Fu, Y. Z. *Anal. Chem.* **2020**, *92*, 12145−12151.
(9) Fang, S.; Lee, H. J.; Wark, A. W.; Corn, R. M. *J. Am. Chem. Soc.* **2006**, *128*, 14044−14046.

(10) Lv, S. Z.; Zhang, K. Y.; Zhu, L.; Tang, D. P. *Anal. Chem.* **2020**, *92*, 1470−1476.
(11) Wang, J.; Lv, W. X.; Wu, J. H.; Li, H. Y.; Li, F. *Anal. Chem.* **2019**, *91*, 13831−13837.
(12) Shu, J.; Tang, D. P. *Anal. Chem.* **2020**, *92*, 363−377.
(13) Long, D.; Li, M. J.; Wang, H. H.; Wang, H. J.; Chai, Y. Q.; Li, Z. H.; Yuan, R. *Anal. Chem.* **2020**, *92*, 14769−14774.
(14) Li, P. P.; Cao, Y.; Mao, C. J.; Jin, B. K.; Zhu, J. J. *Anal. Chem.* **2019**, *91*, 1563−1570.
(15) Zeng, R. J.; Luo, Z. B.; Su, L. S.; Zhang, L. J.; Tang, D. P.; Niessner, R.; Knopp, D. *Anal. Chem.* **2019**, *91*, 2447−2454.
(16) Li, M. J.; Liang, W. B.; Yuan, R.; Chai, Y. Q. *ACS Appl. Mater. Interfaces* **2019**, *11*, 11834−11840.
(17) Mo, F. J.; Wu, J. L.; Chen, M.; Meng, H.; Han, Q.; Fu, Y. Z. *Sens. Actuators, B* **2019**, *289*, 269−276.
(18) Fu, Y. M.; Zou, K.; Liu, M. Y.; Zhang, X. H.; Du, C. C.; Chen, J. H. *Anal. Chem.* **2020**, *92*, 1189−1196.
(19) Mo, F.; Han, M.; Weng, X.; Zhang, Y. Y.; Li, J.; Li, H. B. *Anal. Chem.* **2021**, *93*, 1764−1770.
(20) Fu, Y. M.; Xiao, K.; Zhang, X. H.; Du, C. C.; Chen, J. H. *Anal. Chem.* **2021**, *93*, 1076−1083.
(21) Qian, Y. Y.; Li, D. D.; Han, Y. L.; Jiang, H. L. *J. Am. Chem. Soc.* **2020**, *142*, 20763−20771.
(22) Gong, Y. N.; Zhong, W. H.; Li, Y.; Qiu, Y. Z.; Zheng, L. R.; Jiang, J.; Jiang, H. L. *J. Am. Chem. Soc.* **2020**, *142*, 16723−16731.
(23) Feng, K. Y.; Hao, H. M.; Huang, F. W.; Lang, X. J.; Wang, C. *Mater. Chem. Front.* **2021**, *5*, 2255−2260.
(24) Xie, S. B.; Dong, Y. W.; Yuan, Y. L.; Chai, Y. Q.; Yuan, R. *Anal. Chem.* **2016**, *88*, 5218−5224.
(25) Zhang, Y. H.; Li, M. J.; Wang, H. J.; Yuan, R.; Wei, S. P. *Anal. Chem.* **2019**, *91*, 10864−10869.
(26) Zhang, P.; Jiang, J.; Yuan, R.; Zhuo, Y.; Chai, Y. Q. *J. Am. Chem. Soc.* **2018**, *140*, 9361−9364.
(27) Li, Y.; Chen, F. Z.; Xu, Y. T.; Yu, W. J.; Li, H. Y.; Fan, G. C.; Han, D. M.; Zhao, W. W.; Jiang, D. C. *Anal. Chem.* **2019**, *91*, 12606−12610.
(28) Yang, X. Y.; Gao, Y.; Ji, Z. P.; Zhu, L. B.; Yang, C.; Zhao, Y.; Shu, Y.; Jin, D. Q.; Xu, Q.; Zhao, W. W. *Anal. Chem.* **2019**, *91*, 9356−9360.
(29) Yang, R. Y.; Liu, J. *J. Electroanal. Chem.* **2020**, *873*, No. 114346.
(30) Meng, L. X.; Li, Y. M.; Yang, R. Y.; Zhang, X. H.; Du, C. C.; Chen, J. H. *Chem. Commun.* **2019**, *55*, 2182−2185.
(31) Peng, X.; Wen, Z. B.; Yang, P.; Chai, Y. Q.; Liang, W. B.; Yuan, R. *Anal. Chem.* **2019**, *91*, 14920−14926.
(32) Cheng, Y. Y.; Xie, Y. F.; Li, C. M.; Li, Y. F.; Huang, C. Z. *Anal. Chem.* **2019**, *91*, 11023−11029.
(33) Tang, X.; Deng, R. J.; Sun, Y. P.; Ren, X. J.; Zhou, M. X.; Li, J. H. *Anal. Chem.* **2018**, *90*, 10001−10008.
(34) Lu, J.; Wu, L.; Hu, Y. F.; Wang, S.; Guo, Z. Y. *Biosens. Bioelectron.* **2018**, *109*, 13−19.
(35) Xu, Z. Q.; Liao, L. L.; Chai, Y. Q.; Wang, H. J.; Yuan, R. *Anal. Chem.* **2017**, *89*, 8282−8287.
(36) Tu, W. W.; Cao, H. J.; Zhang, L.; Bao, J. C.; Liu, X. H.; Dai, Z. H. *Anal. Chem.* **2016**, *88*, 10459−10465.
(37) Zhang, N.; Shi, X. M.; Guo, H. Q.; Zhao, X. Z.; Zhao, W. W.; Xu, J. J.; Chen, H. Y. *Anal. Chem.* **2018**, *90*, 11892−11898.

https://doi.org/10.1021/acs.analchem.1c03460
Anal. Chem. 2021, 93, 13727−13733